Low-Temperature Characterization of Lithium-Ion Carbon Anodes via Microperturbation Measurement

Chunsheng Wang,[a,*,z] A. John Appleby,[a,*] and Frank E. Little[b]

*aCenter for Electrochemical Systems and Hydrogen Research and bCenter for Space Power,
Texas Engineering Experiment Station, Texas A&M University, College Station, Texas 77843-3118, USA*

The low-temperature performance limits of Johnson Matthey (JM) 287 graphite and mesocarbon microbead (MCMB) 6-10 coke were investigated using galvanostatic intermittent titration (GITT) and electrochemical impedance spectroscopy. The poor low-temperature ($-30°C$) performance of graphite insertion anodes results from a low lithium insertion capacity because polarization or overpotential is higher than the stage transformation plateau potential. This results in a shorter plateau potential region containing the lithium-rich stages, *e.g.*, $Li_{0.33}C_6$, $Li_{0.5}C_6$, and Li_1C_6. Overall, there is an incomplete transformation from Li-poor to Li-rich stages when the cutoff potential is limited to 0.0 V (*vs.* Li/Li^+) to avoid metallic lithium deposition. The good low-temperature performance of MCMB 6-10 coke is attributed to the smooth change of equilibrium Li content as a function of potential. The high polarization only decreases Li insertion capacity by a small percentage. At room temperature, stage transformation is the rate-controlling step of electrochemical Li insertion-extraction kinetics for JM 287 graphite. However, at $-30°C$ the resistance of solid electrolyte interphase film increases by a factor of over 27, and becomes limiting.
© 2002 The Electrochemical Society. [DOI: 10.1149/1.1474427] All rights reserved.

Lithium-ion batteries are now widely used in civilian applications such as portable telephones and lap-top computers, in which they are typically operated at moderate temperatures and rates. However for aerospace applications, good low-temperature performance and high-power density are required. Generally the cells show poor electrochemical kinetics in power pulses, especially at low temperature ($<-30°C$). Poor low-temperature performance is mainly due to carbon electrode activity,[1,2] which has been attributed to poor solution transport at the solid electrolyte interphase (SEI),[2] high charge-transfer resistance, or low Li diffusivity into carbon,[1] rather than to Li-ion conductivity in liquid electrolytes.[1-3] The different low-temperature rate-controlling mechanisms suggested for carbon anodes based on previous low-temperature studies result from the use of simple galvanostatic charge-discharge measurements of poor diagnostic ability,[1-3] which only give the total reaction resistance. More powerful diagnostic techniques are therefore needed for investigating the reactions.

Micropertubation techniques such as electrochemical impedance spectroscopy (EIS) and galvanostatic intermittent titration (GITT) with microcurrent are effective for the determination of reaction kinetics. EIS can give individual reaction resistances for each step if their time constants are resolvable, and therefore may be used to determine the reaction kinetics for electrochemical Li insertion into carbon as a function of temperature.[4,5] GITT can give the equilibrium potential and total reaction resistance for lithium insertion-extraction as a function of lithium content if the current is small and the relaxation time is sufficiently long for the equilibrium potential to be attained.[4] In this work, the kinetics of Li insertion-extraction into Johnson Matthey (JM) 287 graphite and mesocarbon microbead (MCMB) 6-10 coke at room and low-temperature ($-30°C$) have been investigated using EIS and GITT.

Experimental

Electrode and cell preparation.—JM 287 graphite powder (Johnson-Matthey, particle diameter *ca.* 15 μm, Brunauer-Emmett-Teller (BET) area >13.5 m² g⁻¹) and MCMB 6-10 coke (*ca.* 6 μm, 3.23 m² g⁻¹) were used as intercalation anode materials. Composite graphite electrodes sandwiched between two nickel screen current collectors were prepared as in previous work from a mixture of 80 wt % JM 287 (*ca.* 50 mg) with 10 wt % each of carbon black and polyvinylidene fluoride binder in 1-methyl-2-pyrrolidinone solvent. However, 92 wt % MCMB 6-10 (*ca.* 80 mg) with 8 wt % polyvi-

nylidene fluoride binder in 1-methyl-2-pyrrolidinone solvent was used to prepare the coke electrode. After drying overnight at 110°C, the 2.0 cm² geometric area, 0.8 mm thick electrodes were pressed to the configuration shown previously.[4,5] Electrochemical measurements were conducted in a three-electrode polytetrafluoroethylene (PTFE) cell. Two lithium foils were used as both counter and reference electrodes. All potentials given are *vs.* the Li/Li^+ reference electrode in the electrolyte used, *i.e.*, 1.0 M lithium hexafluorophosphate ($LiPF_6$) in a 4:1:3:2 by volume ethylene carbonate (EC)-propylene carbonate (PC)-dimethylcarbonate (DMC)-ethyl methyl carbonate (EMC) mixture (high purity lithium battery grade, Mitsubishi Chemical Company). To determine the solidification temperature of the electrolyte, a sample was sealed in a glass tube in a glove box, then exposed for 3 days at $-20°C$, then at $-30°C$. The above electrolyte remained completely liquid at $-20°C$, and only a small amount of the solid phase at the bottom of the tube was observed at $-30°C$.

Electrochemical cells were assembled in an argon-filled glove box. Charge (lithium intercalation) and discharge (lithium extraction) characteristics were measured between +0.0 and +1.5 V at constant current using an Arbin Instruments (College Station, TX) automatic battery cycler. The graphite sandwich electrode was charged/discharged on one side only, and the intrinsic resistance of the electrode was approximately calculated from the ratio of trans-electrode voltage to the dc current passed (10 mA for JM 287, 1 mA for MCMB 6-10).[4,5] Two identical JM 287 graphite anodes (JM1 and 2) and one MCMB 6-10 coke anode were used. The JM1 anode was first charged-discharged at 25°C for two cycles using GITT as a series of intermittent charges or discharges at 5 mA/g for 4 h with the electrode at open circuit for 2.0 h between each. Its reaction and intrinsic impedances were then measured during the third charge to 200, 115, and 75 mV. After discharge to 1.5 V, it was cooled and maintained at $-30°C$ for 2 days. Its EIS were then taken on charge to the above three potentials, and its rate capability then determined. The JM2 anode was first charge-discharged at $-30°C$ for two complete cycles under GITT conditions at 2 mA/g in the first cycle and 0.8 mA/g in the second cycle for 4 h each, with 2.0 h on open circuit between each. Its EIS were measured in the third charge to 200, 115, and 75 mV. After discharge to 1.5 V, it was heated and maintained at 25°C for 2 days, and its EIS was again taken on charge to the same potentials. The MCMB 6-10 coke anode was GITT charge-discharged at $-30°C$ at a current of 0.7 mA/g for 4 h, with 2 h at open circuit between each charge in the first and third complete

cycles. However, it was given normal galvanostatic charge-discharge at 0.7 mA/g at $-30°C$ in the second cycle. In the fourth charge to 75 mV at $-30°C$, its reaction and intrinsic impedances were measured by EIS, following which its rate capability was measured at $-30°C$.

GITT measurements.—Lithium was inserted into or extracted from the graphite anode in a series of intermittent charges or discharges at the above mentioned current for 4.0 h, the electrode being held at open circuit for 2.0 h between each charge/discharge. The potential was logged at regular time intervals by computerized data acquisition. The total reaction resistance of lithium insertion-extraction as a function of lithium content was directly calculated from the ratio of overpotential to charge-discharge current since the intermittent currents were small and the 2.0 h of relaxation time was sufficiently long for an effective equilibrium potential to be attained. The intrinsic resistance at different Li content was calculated from the ratio of trans-electrode voltage to the dc current passed.

EIS measurements.—In each case, this was taken over the 65 kHz to 1.0 mHz frequency range at a potentiostatic signal amplitude of 5 mV, using a Solartron 1250 frequency response analyzer (FRA) and a Solatron model 1286 electrochemical interface. Measurements were performed after electrodes were left on open circuit for 2 h for potential stabilization. For electrochemical reaction kinetic measurement, the signal was applied to the current collector on both sides of the electrode. For intrinsic resistance measurements, the EIS was measured between the two sides. All reactions and intrinsic resistances, whether measured from EIS or GITT, were normalized to the weight of the electrode. Fitting of impedance spectra to the proposed equivalent circuit was performed by using the code Z_{view} (Version 1.4, Scribner Associate, Inc.).

Results and Discussion

GITT and intrinsic resistance measurement of JM 287 anodes during the first and second charge-discharge cycles at 25 and $-30°C$.—GITT was applied to JM 287 anodes at 25 and $-30°C$ to investigate the reaction kinetics and intrinsic resistance during the first and second Li insertion-extraction cycle. This procedure was used because a pronounced increase in the cycle life of graphite anodes was observed when the passive SEI layer was formed at low temperatures.[6] Figure 1 shows the typical potential and intrinsic resistance as a function of capacity for the first and second charge-discharge cycles of the JM1 anode at 25°C under GITT conditions. The open-circuit potential, reaction and intrinsic resistances of the material at different Li insertion-extraction levels in the first and second charge-discharge cycles at 25°C (JM1) and $-30°C$ (JM2) are shown in Fig. 2. Previous reaction resistance study using GITT measurements at 25°C showed that 2 h of relaxation time after intermittent charge-discharge at 5.1 mA/g is sufficiently long for JM 287 graphite to reach equilibrium potential.[4] However, this may not be true at $-30°C$ when the reaction resistance is over ten times higher. Therefore, an intermittent current of 2.0 mA/g at $-30°C$ was used instead of the 5 mA/g value at 25°C. Although a 2.0 h relaxation time with 4.0 h, 2.0 mA/g intermittent charge/discharge conditions may still be insufficient to reach true equilibrium at temperature under $-30°C$, the reaction resistance as measured is nevertheless very useful for a relative comparison of the reaction kinetics at different temperatures and different Li insertion levels in the first cycle. A further decrease in the GITT current or a further increase in the relaxation time in the first Li insertion-extraction cycle at $-30°C$ is limited by the time required to fully charge the electrode to 0.0 V to 450 mAh/g (Fig. 2a) under this regime. This is because the continued growth of the SEI film during the first cycle, which makes results obtained at long times sufficiently different to prevent direct comparison. A final problem with long total charging times is the increasing anode self-discharge. Because the capacity in the second cycle is much smaller (220 mAh/g), the current for the JM2 anode was decreased to 0.8 mA/g to more closely approach the
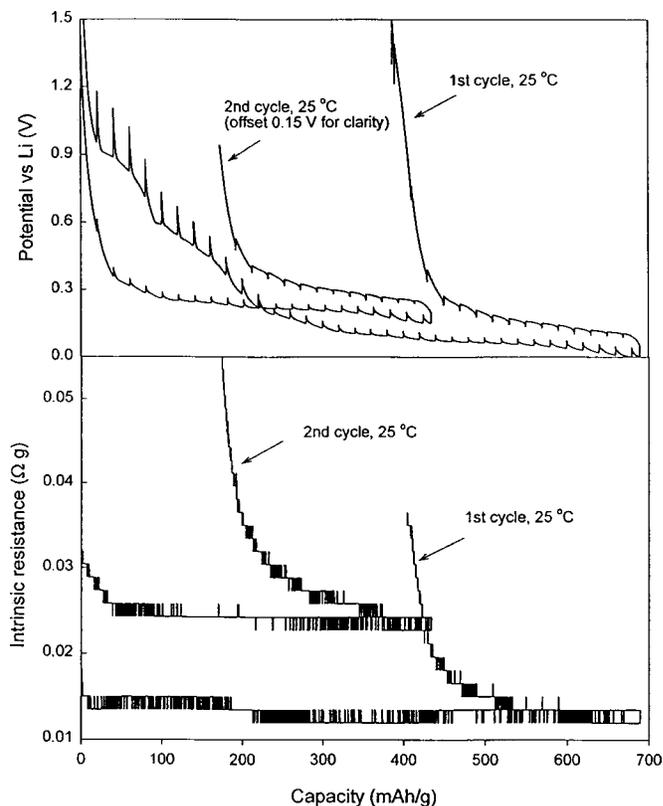

Figure 1. Typical electrode potential and intrinsic resistance as a function of capacity for the first and second charge-discharge cycles for JM 287 anodes at 25°C from GITT measurements. Charge-discharge current, 5.0 mA/g for 4.0 h, followed by 2.0 h relaxation. Current for intrinsic resistance measurement: 10 mA.

equilibrium potential and give a more accurate reaction resistance. More accurate reaction kinetics investigated by EIS are given in a later section and compared with GITT results. The results shown in Fig. 1 and 2 may be summarized as follows

1. At 25°C, the reaction resistance of anode JM1 during the first charge from 1.0 to 0.2 V behaved in a manner similar to the open-circuit potential (Fig. 2a), and the overpotential in the first charge from 1.0 to 0.2 V was higher than that in the second charge (Fig. 1). This result suggests that the solvent co-insertion and SEI film formation controls the reaction rate for initial Li insertion. As was previously suggested,[7] the two potential plateaus at around 1.0 and 0.7 V during initial Li insertion into the JM1 anode resulted from a combination of solvent co-insertion and electrolyte decomposition (*i.e.*, SEI formation). Below 0.2 V, the reaction resistance shows a typical stage transformation character, *i.e.* gradually increasing in the potential plateau region, then falling in the single-phase region.[7]

2. At $-30°C$, the open-circuit potential plateau at around 1.0 V during the first charge cycle became lower and flatter, and the reaction resistance gradually increased as Li insertion proceeds in the potential plateau region, corresponding to typical stage transformation (Fig. 2a). This suggests that at low temperatures, electrolyte decomposition is slightly reduced, but solvent co-intercalation is not inhibited and induces a large increase in intrinsic resistance, as Fig. 2a shows.

3. The temperature has little influence on the initial charge (Li insertion) capacity of JM 287 graphite anode above 0.2 V (Fig. 2a). Similar behavior was also reported for the initial charge of an MCMB6-28 anode in an EC-EMC (1:4) solution at 20 and at $-20°C$.[8] However, the discharge (Li extraction) capacity at $-30°C$ is considerably less than that at 25°C even at the low charge-discharge current of 2 mA/g compared with 5 mA/g at 25°C. This
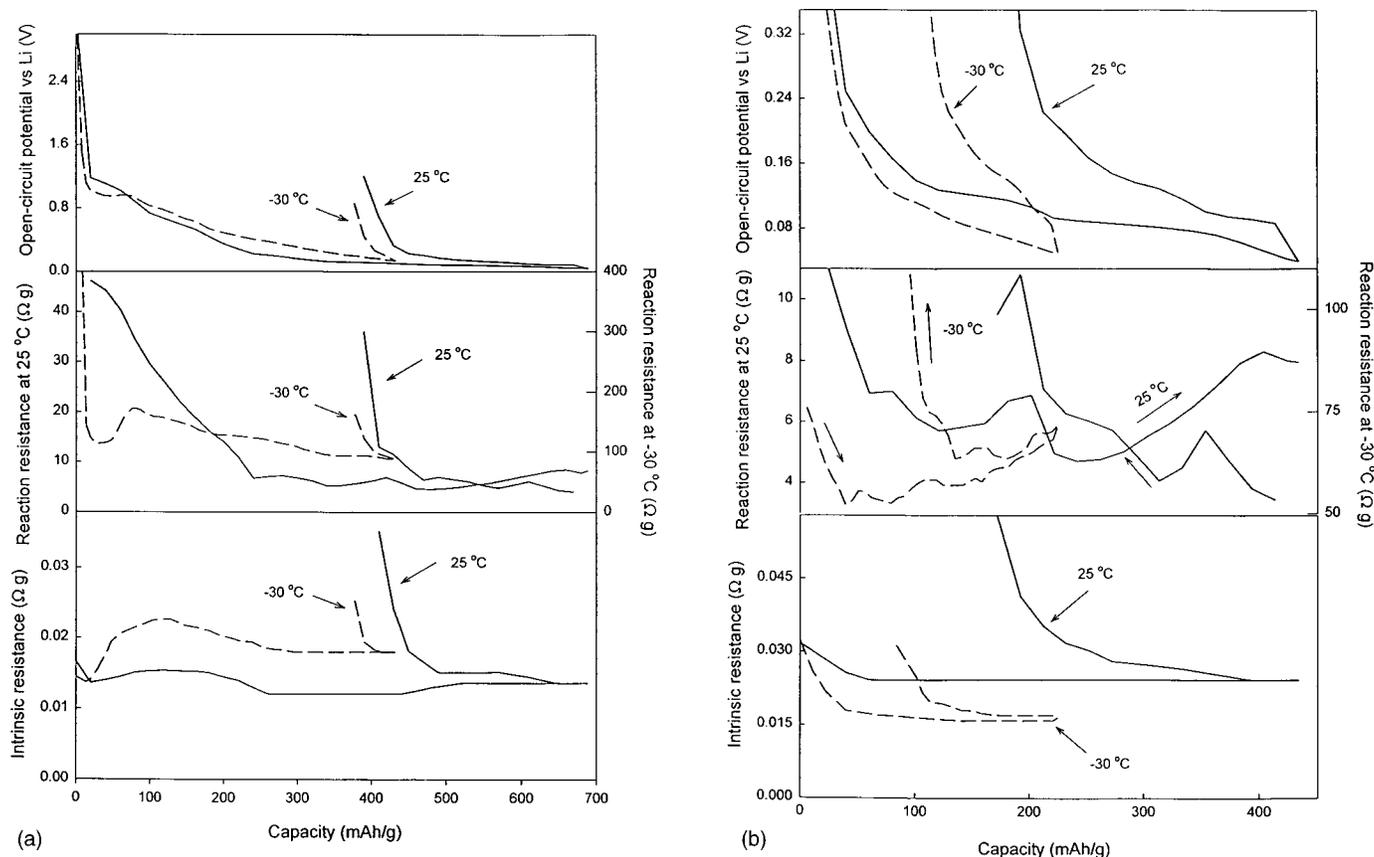
Figure 2. Dependence of open-circuit potential, reaction resistance, and intrinsic resistance for JM 287 anodes on Li content in the (a) first and (b) second GITT charge-discharge cycles at 25°C and −30°C. Charge-discharge current at 25°C, 5.0 mA/g, at −30°C, 2.0 mA/g in the first cycle, 0.8 mA/g in the second cycle. Intermittent current imposed for 4.0 h, followed by 2.0 h relaxation. Current for intrinsic resistance measurement: 10 mA.

results from the large Li insertion polarization, limiting Li insertion to only $Li_{0.2}C_6$, as is shown by the 170 mV open-circuit potential at the end of charge (Fig. 2a), which is higher than the 117 mV[9] equilibrium potential between the $Li_{0.33}C_6$ and $Li_{0.5}C_6$ and the 81 mv[9] equilibrium potential between $Li_{0.5}C_6$ and LiC_6 (assuming that little change of these potentials with temperature occurs).[9] In other words, the high polarization of the insertion reaction limits Li insertion capacity on charging to 0.0 V, because this potential cannot be cathodically exceeded to avoid metallic lithium deposition. Almost 66% of the total Li at full charge is stored in graphite in the last two stage transformations at potentials from +117 mV to 0.0 V. This high polarization corresponded to a reaction resistance at least 15 times higher than that at 25°C (Fig. 2a). If the low extraction capacity results from a high Li insertion polarization as discussed above, decreasing the Li insertion current should increase the Li insertion and extraction capacity. As expected, the Li extraction capacity during the second cycle with a low (0.8 A/g) intermittent charge-discharge current increased to 142 mA/g ($Li_{0.38}C_6$) at −30°C (Fig. 2b). An important result from Fig. 2b is that the anode reaction resistance for Li insertion at −30°C is similar to that for Li extraction. The reaction resistance measured by GITT is the sum of resistances for the electrolyte, SEI film, charge-transfer, stage transformation, and Li diffusion in graphite.[4] The first three resistances are all similar during insertion and extraction,[1] so the similarity of the corresponding reaction resistances suggests that the concentration resistances are also similar, provided that the corresponding stage transformation resistances are also comparable. This differs from previous suggestions that the concentration dependence of Li diffusivity would result in higher concentration polarization insertion compared with extraction, giving a low Li insertion capacity.[1] Previous work[1] showed that the increase in polarization resulting from

a change in temperature from 25 to −40°C was *ca.* 600 mV at a Li extraction current of 0.285 mA/cm². If the Li insertion polarization is the same as that for extraction, the corresponding 600 mV overpotential would be much higher than the total potential range (<200 mV) for all three stage transformations, which would result in almost zero Li insertion capacity.

4. Three potential plateaus and three reaction peaks for the JM 287 anode cycling at −30°C can be observed in Fig. 2b, although they are not as prominent as at 25°C. While a horizontal baseline for reaction resistance is observed at 25°C, at −30°C it increased with Li content. This may be satisfactorily explained using the shrinking unreacted core model. For example, during Li insertion into graphite, the Li-poor phase $Li_{0.33}C_6$ is covered by a Li-rich phase, $Li_{0.5}C_6$, at potentials around 117 mV. As the phase boundary between $Li_{0.5}C_6$ and $Li_{0.33}C_6$ moves towards the particle center, the Li diffusion length gradually increases, giving an increase in concentration polarization. When the potential is lower than the equilibrium potential between $Li_{0.5}C_6$ and Li_1C_6, the new Li_1C_6 covers the second ($Li_{0.5}C_6$) layer, even though some $Li_{0.33}C_6$ still exists in the core. The phase transformations involving the three phases increase the reaction resistance, and potential does not go back to the original value even when the $Li_{0.33}C_6$ core disappears. This is because the $Li_{0.5}C_6$ to Li_1C_6 phase transformation and concentration polarizations are still present. The incomplete stage transformation limits the overall capacity, and results in an increase in the reaction resistance baseline with increasing Li content, as Fig. 2b shows.

The above analysis suggests that the limited low-temperature performance of graphite anodes may be largely attributed to the existence of a higher polarization or overpotential than the stage transformation plateau potential, limiting the amount of Li insertion,
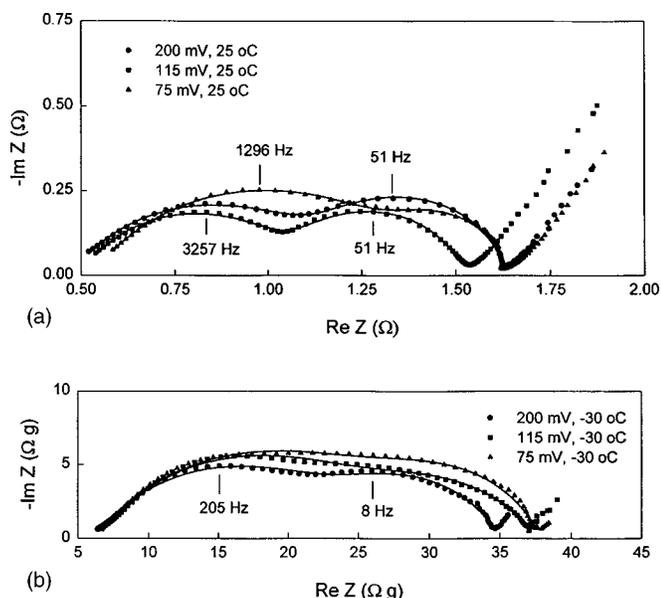
(a)

(b)

Figure 3. Nyquist plots for reaction kinetic impedance measured at 200, 115, and 75 mV during (a) third Li insertion into JM 287 anode (JM1) at 25°C and (b) fourth Li insertion at −30°C. Before measurement, electrode subjected to 2 GITT cycles at 25°C, *i.e.*, charge/discharge at 5.0 mA/g for 4.0 h, followed by 2.0 h relaxation. Solid line: fitted results from the equivalent circuit in Fig. 5 obtained using the code Zview (version 1.4, Scribner Associate, Inc.).

(a)

(b)

Figure 4. Nyquist plots for reaction kinetics impedance measured at 200, 115, and 75 mV during (a) third Li insertion into JM 287 anode (JM2) at −30°C and (b) fourth Li insertion, conducted at 25°C. Before measurement, electrode subjected to 2 GIT cycles at −30°C, *i.e.*, charge-discharge at 0.8 mA/g for 4.0 h, followed by 2.0 h relaxation. Solid lines: fitted results from the equivalent circuit in Fig. 5 obtained using the code Zview (version 1.4, Scribner Associate, Inc.).

and thus the extraction capacity. This low-temperature behavior may be improved by increasing the Li insertion-extraction kinetics at low temperatures, *e.g.*, by measuring the reaction resistance change from 25 to −30°C, and determining the rate-controlling step using EIS, and then finding a means of decreasing its reaction resistance. To examine the limiting step at low temperatures, EIS was applied to the graphite anodes at 25 and −30°C.

EIS measurement of JM 287 graphite anodes at 25 and −30°C.—After two GITT charge-discharge cycles at 25°C (JM1) and at −30°C (JM2), the reaction and intrinsic (strictly speaking, transmissive) impedances were measured under the conditions indicated earlier. To investigate the effect of precycling temperature on subsequent reaction kinetics, the temperatures of the JM1 and JM2 electrodes were switched before the fourth cycle (see Experimental section). The reaction impedance and intrinsic impedance were then measured again at 0.2, 0.115, and 0.075 V, following a 2.0 h relaxation time. Figure 3 shows reaction kinetic impedance of JM1 during the third charge to 200, 115, and 75 mV at 25°C, and during the fourth charge to the same potentials at −30°C. Figure 4 shows the same data of the JM2 electrode on the third charge at −30°C, and on the fourth charge at 25°C. The impedances in Fig. 3 and 4 are typical of the graphite electrode, *i.e.*, two separate depressed semicircles in the high frequency range with a linear portion at low frequency. However, the latter were merged into a single depressed semicircle in Fig. 4b. The depressed semicircle at high frequency is attributed to the SEI film, and the second semicircle in the middle frequency region is ascribed to the charge-transfer reaction. The linear portion at low-frequency is characteristic of Li diffusion in graphite. The intersection of the high-frequency line with the real axis is the electrolyte resistance from the reference electrode to the graphite electrode, including the part within its porosity. The measured electrolyte resistance changed slightly with potential, which may be attributed to changes in anode surface area and pore diameter. On switching the temperature from 25 to −30°C for JM1 in Fig. 3, and from −30 to 25°C for JM2 in Fig. 4, the two depressed semicircles tended to overlap (Fig. 3b) or even merge into a single
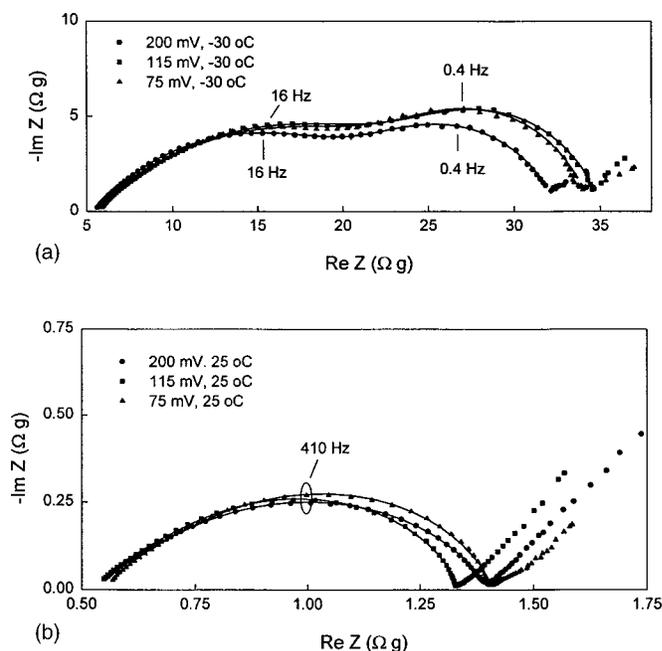
depressed semicircle (Fig. 4b). This result suggests that the effects of temperature on the SEI film and charge-transfer impedances are different. To analyze the influence of temperature on reaction kinetics, the EIS values in Fig. 3 and 4 were fitted using the equivalent circuit shown in Fig. 5.[10] In Fig. 5, the constant phase elements Q_{SEI} and Q_{ct} are put in parallel with R_{SEI} and R_{ct} to fit the depressed SEI film and charge-transfer semicircle, respectively. The Q_w is a constant phase element to simulate the Warburg impedance.[11] The general expression for the admittance response of the constant phase element (CPE) is[11]

$$Y_{CPE} = Y_c \omega^n \cos(n\pi/2) + iY_c \omega^n \sin(n\pi/2)$$

where ω is the angular frequency, and $i = (-1)^{1/2}$. Depending on the value of n, the CPE can have a variety of responses. If $n = 0$, it represents a resistance with $R = Y_c^{-1}$; if $n = 1$, a capacitance with $C = Y_c$, and if $n = 0.5$, a Warburg impedance.

Since the Warburg impedance at −30°C shows some noise, the linear portion in the low-frequency region was not simulated (*i.e.*, $Q_w = 0$).

The fitted impedances using the proposed equivalent circuit described the two depressed semicircles satisfactorily for different temperatures and potentials, as is shown by the solid lines in Fig. 3 and 4, and the fitted parameters are listed in Table I.
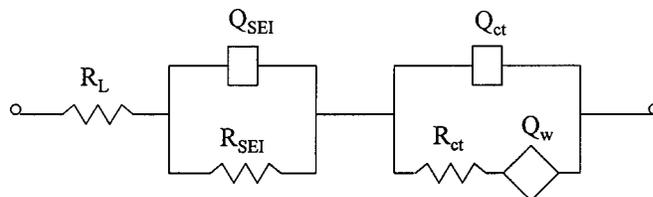

Figure 5. Equivalent circuit of reaction impedance for Li-ion battery anode.

Table I. Parameter values obtained from experimental impedance spectra of JM 287 graphite electrodes at 25 and −30°C.

Sample		25°C			−30°C			$R_{(-30)}/R_{(25)}$
		200 mV	115 mV	75 mV	200 mV	115 mV	75 mV	
JM1	R_L (Ω g)	0.48	0.5	0.53	6.11	6.35	6.12	12.3
	R_{SEI} (Ω g)	0.69	0.57	0.88	18.04	19.47	22	27.8
	R_{ct} (Ω g)	0.47	0.45	0.22	10.73	11.62	9.84	28.24
	Y_{SEI} (μF)	0.12	0.08	0.12	0.04	0.04	0.05	
	Y_{ct} (μF)	0.82	1.4	0.4	0.8	0.82	0.6	
	n_{SEI}	0.66	0.7	0.64	0.58	0.59	0.58	
	n_{ct}	0.88	0.83	1	0.7	0.62	0.74	
	ΣR	1.64	1.52	1.63	34.88	37.44	37.96	23.02
JM2	R_L (Ω g)	0.54	0.53	0.55	5.44	5.62	5.5	10.22
	R_{SEI} (Ω g)	0.66	0.6	0.63	17.2	21.2	21.3	31.6
	R_{ct} (Ω g)	0.21	0.21	0.233	10	8.55	8.06	40.75
	Y_{SEI} (μF)	0.22	0.12	0.13	0.19	0.3	0.34	
	Y_{ct} (μF)	0.23	0.31	0.29	3.3	4.7	5.2	
	n_{SEI}	0.72	0.82	0.82	0.53	0.5	0.48	
	n_{ct}	0.71	0.66	0.67	0.78	0.9	0.91	
	ΣR	1.41	1.34	1.413	32.64	35.37	34.86	24.71

JM1: after two GIT cycles at 25°C, EIS conducted on JM1 anode during the third charge at 25°C and during the fourth charge, conducted at −30°C.
JM2: after two GIT cycles at −30°C, EIS conducted on JM2 anode during the third charge at −30°C and during the fourth charge, conducted at 25°C.
$R_{(-30)}/R_{(25)}$: average resistance ratio at −30°C to that at 25°C; $R_{(-30)}$: average resistance at three potentials (200, 1115, and 75 mV), −30°C; $R_{(25)}$: average resistance at the same potentials, 25°C.

The phase transformation resistance is not included in the experimental EIS results because the small 5 mV potentiostatic signal amplitude results in an essentially constant state of charge during the measurements. However, it is included in the total reaction resistance measured from GITT, so it may be derived from the difference between the two.[7] Table I shows that the sum of the electrolyte, SEI film, and charge-transfer resistances for the JM1 anode at 25°C is around 1.52-1.64 Ω g. The baseline total reaction resistance (except that for Li diffusion) measured via GITT was around 5 Ω g (Fig. 2b). Hence the JM1 anode stage transformation resistance is around 3.26-3.48 Ω g. The JM1 resistances at 25°C in decreasing order were; stage transformation (3.26-3.48 Ω g) > SEI film (0.57-0.88 Ω g) > electrolyte (0.48-0.53 Ω g) > charge-transfer (0.22-0.47 Ω g). The diffusion resistance changes from 0 to 3 Ω g (Fig. 2b). Thus, stage transformation is the rate-controlling step for JM 287 graphite anodes at 25°C.

If it is considered that the open-circuit potential following 2 h relaxation after intermittent charge-discharge at 0.8 mA/g approximates to the equilibrium potential, the phase transformation resistance at −30°C can be estimated from the first stage transformation at 0.2 V under conditions where no multiple phases coexist. The total reaction resistance at −30°C at the start of stage transformation at 0.2 V is *ca.* 50 Ω g (Fig. 2b), and the sum of the electrolyte, SEI film, and charge-transfer resistances is 32.6-35.4 Ω g (Table I). Therefore the stage transformation resistance is around 14.6-17.4 Ω g. Hence the resistances for JM 287 anodes at −30°C in decreasing order are SEI (17.2-21.3 Ω g) > stage transformation (14.6-17.4 Ω g) > charge-transfer (8.1-10.0 Ω g) > electrolyte (5.4-5.5 Ω g). From this analysis, the key to improving the low-temperature performance of graphite anodes is to decrease the low-temperature SEI film, stage transformation, and charge-transfer resistances so that the anode polarization at the desired charge-discharge current is lower than the equilibrium potential difference between $Li_{0.5}C_6$ and Li_1C_6, *i.e.*, 75 mV. The EC-PC-DMC-EMC electrolyte does not limit low-temperature graphite anode performance even through some solid phase was observed in the EC-PC-DMC-EMC electrolyte at −30°C, in agreement with previous analyses.[1,3]

When the temperature was decreased from 25 to −30°C, electrolyte resistance only increased 10-12 times. In contrast, the corresponding SEI film and charge-transfer resistances increased 27-28 times over this temperature range. Moreover, Fig. 3 and 4 and Table I show that precycling at −30°C decreases the charge-transfer resistance only slightly in subsequent cycling at 25°C. In addition, intrinsic resistances measured using EIS at both 25 and −30°C show pure electronic resistance characteristics, whose values are shown in Table II. Table II and Fig. 2 shows that temperature has no obvious influence on the intrinsic resistance.

GITT and intrinsic resistance measurement of MCMB 6-10 coke anode during the first and third charge-discharge cycles at −30°C.—As discussed earlier, the poor low-temperature performance of graphite is limited by a higher polarization than that of the stage transformation plateau potential. This limits the amount of Li insertion, thus the extraction capacity. This poor low-temperature behavior may be improved by using a coke which shows no phase transformation during Li insertion-extraction. For such coke anodes, the equilibrium Li carbon content smoothly increases with decreasing equilibrium potential, and no phase transformation resistance exists during Li insertion-extraction. Figure 6 shows the potential and intrinsic resistance as a function of capacity for the first GITT charge-discharge cycles of the MCMB coke anode at −30°C. The open-circuit potential, reaction, and intrinsic resistances of MCMB coke at different Li insertion-extraction levels in the first and third charge-discharge cycles at −30°C are shown in Fig. 7. A low cur-

Table II. Intrinsic resistance obtained from experimental impedance spectra of JM 287 graphite electrode at 25 and −30°C.

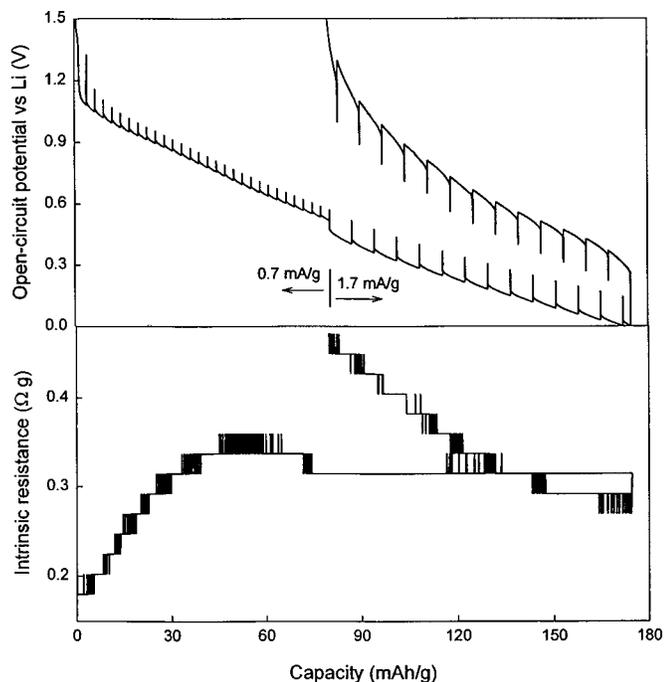| Potential (mV)	Intrinsic resistance (Ω g)	
	25°C	−30°C
200	0.028	0.026
115	0.025	0.024
75	0.022	0.022

Figure 6. Potential and intrinsic resistance as a function of capacity for the first GITT charge-discharge cycles for MCMB 6-10 anodes at −30°C. Charge-discharge current: 0.7 mA/g, then 1.7 mA/g after 80 mAh/g in first cycle, 0.7 mA/g in the third cycle. Intermittent current imposed for 4.0 h, followed by 2.0 h relaxation. Current for intrinsic resistance measurement: 1.0 mA.
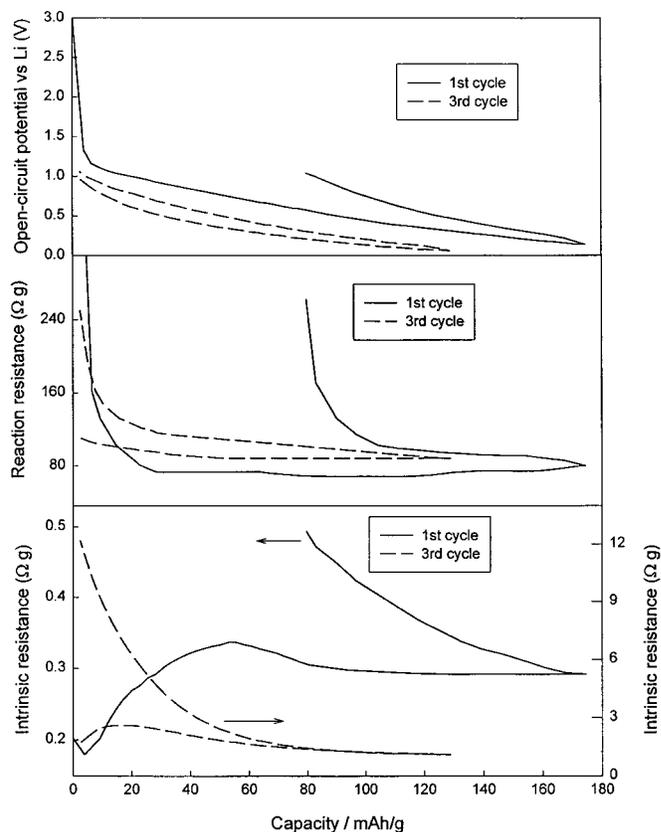

Figure 7. Dependence of open-circuit potential, reaction resistance, and intrinsic resistance for MCMB 6-10 anode on Li content in the first and third GIT charge-discharge cycles at −30°C. Charge-discharge current during first cycle initially 0.7 mA/g, increased to 1.7 mA/g after 80 mAh/g, then maintained at 0.7 mA/g during second cycle. Intermittent current imposed for 4.0 h, followed by 2.0 h relaxation. Current for intrinsic resistance measurement: 1.0 mA.
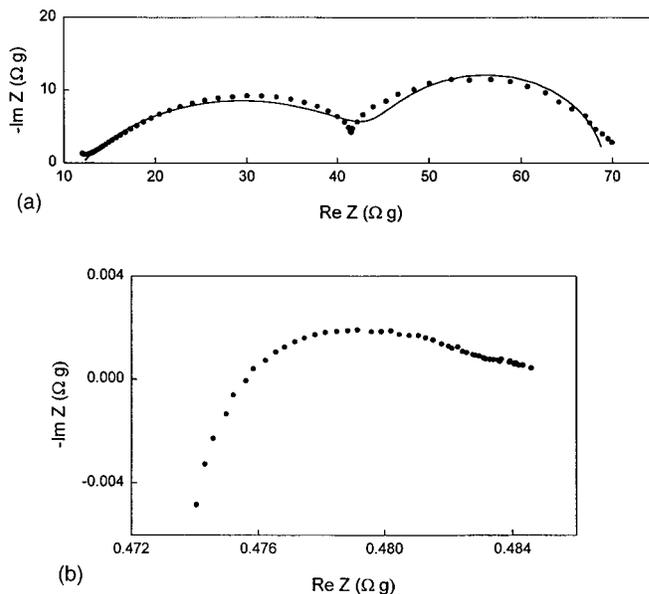
rent density (0.7 mA/g) was used in order to achieve the equilibrium potential after 2.0 h of relaxation. To verify whether this value is sufficiently low to attain equilibrium after 2.0 h relaxation time, the Li insertion current was increased from 0.7 to 1.7 mA/g after 80 mAh/g (Fig. 6). No reaction resistance change was observed on changing the current (Fig. 7), so the relaxation time used is sufficient to reach equilibrium under these conditions. From a comparison of Fig. 2 and 7 the differences between MCMB coke and JM 287 graphite anodes may be summarized as follows

1. Figure 7 shows that the open-circuit potential of the MCMB 6-10 anode decreases gradually with Li insertion capacity in both the first and third charge-discharge cycles at −30°C. No potential plateaus or reaction resistance peaks related to solvent coinsertion and stage transformation were observed in these cycles. In the first discharge cycle, the reaction resistance of MCMB 6-10 is similar to or slightly higher than that of JM 287 and its first Li insertion capacity is much less. However its Li extraction capacity is much higher than that of JM graphite, as a comparison of Fig. 2 and 7 shows. This result confirms the hypothesis that the ratio of the overpotential to the plateau potential of the Li-rich phase controls the low-temperature performance of carbon anodes.

2. The irreversible capacity of the MCMB 6-10 anode attributed to SEI formation in the first charge-discharge cycle is 95 mA/g (Fig. 7). The change of intrinsic resistance seen before 80 mAh/g cannot be explained by SEI formation because it is still seen in the third charge-discharge cycle, where the electrode is almost completely reversible (Fig. 7). The intrinsic resistance peaks appeared at around 0.6 V in both the first and third cycles (Fig. 7), which suggests that the Li storage mechanisms above and below 0.6 V may be different.

3. The intrinsic resistance of MCMB 6-10 at −30°C is at least ten times higher than that of JM 287 at the same temperature (Fig. 2 and 7), and it increases quickly on charge-discharge cycling.

EIS measurement of the MCMB 6-10 coke anode at −30°C.—Figure 8 shows the EIS reaction and intrinsic impedances

Figure 8. (a) Reaction and (b) intrinsic impedances of MCMB 6-10 electrodes on the fourth charge to 75 mV at −30°C. Before measurement, the electrode was subjected to two GITT cycles and one galvanostatic charge-discharge cycle at −30°C.
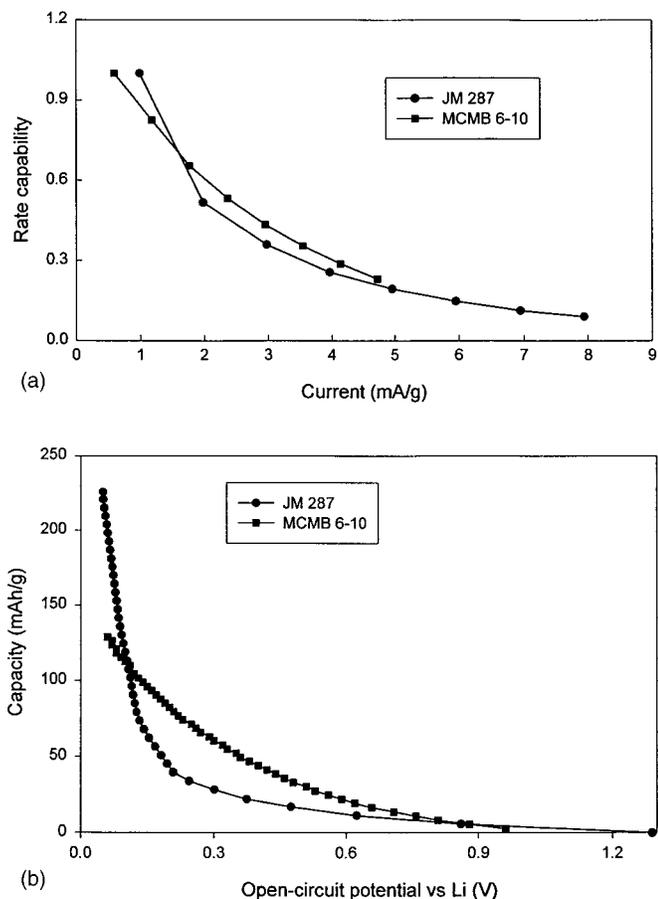
Figure 9. (a) Li insertion rate capability and (b) variation of Li insertion capacity with open-circuit potential for JM 287 and MCMB 6-10 anodes at $-30°$C.

of MCMB 6-10 anode at $-30°$C obtained on the fourth charge to 0.075 V, after 2.0 h relaxation. As with graphite, the reaction impedance shows two depressed semicircles in the high frequency region, representing the SEI film and charge-transfer impedances. The sloping line in the low frequency region showed a great deal of noise and is not shown in Fig. 8a. The line showing the reaction impedance in Fig. 8a was fitted using equivalent circuit in Fig. 5. The SEI film, charge-transfer, and electrolyte resistances were 34.1, 23, and 12 Ω g, respectively. The total reaction resistance at 0.075 V obtained via GITT is *ca.* 85 Ω g (Fig. 7). Hence, the Li diffusion resistance is *ca.* 15 Ω g. Therefore, the rate-determining process for MCMB 6-10 anodes at $-30°$C is the SEI film resistance at 34.1 Ω g, which is almost double the value for JM 287 anodes. Unlike JM

287, the intrinsic impedance of MCMB 6-10 coke shows a depressed semicircle, which suggests that SEI film formation between the carbon particles takes place (Fig. 8b).

Rate capability of JM 287 graphite and MCMB 6-10 coke anodes at $-30°$C.—The rate capability for Li insertion into JM 287 graphite and MCMB 6-10 coke anodes at $-30°$C was measured and is shown in Fig. 9a. As the current increases, rate capability for JM 287 graphite first decreases more rapidly than that of MCMB 6-10 coke, after which the rates become similar. The insertion rate capability as a function of normalized current for both JM 287 and MCMB 6-10 (Fig. 9a) is similar to the behavior of the Li insertion capacity change with open-circuit potential (Fig. 9b). This result again confirms that the limiting low-temperature Li insertion capacity may be attributed to the low plateau potential.

Conclusions

This electrochemical impedance spectroscopy (EIS) and galvanostatic intermittent titration (GITT) study of the low-temperature performance of JM 287 graphite and MCMB coke anodes shows that the limited Li insertion into graphite at $-30°$C may be largely attributed to the fact that its polarization, *i.e.*, overpotential, is larger than the equilibrium plateau potential for the Li-rich phase. This results in incomplete stage transformation and a low Li insertion capacity. The high polarization in both cases is mainly caused by the high SEI film resistance, which is more than 27 times higher at $-30°$C compared with the value at 25°C. In contrast, the resistivity of the liquid electrolyte shows only a 10-fold increase on going from 25 to $-30°$C. Initial precycling of the anodes at low temperature increases the reaction kinetics at room temperature only marginally.

References

1. C.-K. Huang, J. S. Sakamoto, J. Wolfenstine, and S. Surampudi, *J. Electrochem. Soc.,* **147**, 2893 (2000).
2. H.-P. Lin, D. Chua, M. Salomon, H.-C. Shiao, M. Hendrickson, E. Plichta, and S. Slane, *Electrochem. Solid-State Lett.,* **4**, A71 (2001).
3. F. Puglia, R. Gitzendanner, C. Marsh, and T. Curran, *J. Power Sources,* **96**, 40 (2001).
4. C. Wang, I. Kakwan, A. J. Appleby, and F. E. Little, *J. Electroanal. Chem.,* **489**, 55 (2000).
5. C. Wang, A. J. Appleby, and F. E. Little, *Electrochim. Acta,* **46**, 1793 (2001).
6. D. Aurbach, Y. Ein Eli, O. Chusid, Y. Carmeli, M. Babai, and H. Yamin, *J. Electrochem. Soc.,* **141**, 603 (1994).
7. C. Wang, I. Kakwan, A. J. Appleby, and F. E. Little, *J. Electroanal. Chem.,* **489**, 55 (2000).
8. E. Barsoukov, J. H. Kim, J. H. Kim, C. O. Yoon, and H. Lee, *J. Electrochem. Soc.,* **145**, 2711 (1998).
9. T. Ohzuku, Y. Iwakashi, and K. Sawai, *J. Electrochem. Soc.,* **140**, 2490 (1993).
10. T. Piao, S. M. Park, C. H. Doh, and S. I. Moon, *J. Electrochem. Soc.,* **146**, 2794 (1999).
11. B. A. Boukamp, *Equivalent Circuit User's Manual*, 2nd ed., University of Twente, Eindhoven, The Netherlands (1989).